Debonding Evolution in Nonlinear FRP-retrofitted RC Beams with Cohesive Interface

Razaqpur AG[(1,*)], Lamberti M[(2)], Ascione F[(3)]

(1) College of Environmental Science and Engineering, Nankai University, Tianjin, China, email: *GRazaqpur@nankai.edu.cn*
(2) College of Environmental Science and Engineering, Nankai University, Tianjin, China, email: *mlamberti@nankai.edu.cn*
(3) Dept. of Civil Engineering, University of Salerno, Italy, email*: fascione @unisa.it*

**Corresponding author*

This is a post-peer-review, pre-copyedit version of an article published in [Construction and Building Material]. The final authenticated version is available online at: https://doi.org/10.1016/j.compstruct.2021.113591.

Abstract

A novel semi-analytical formulation of the governing equations of an FRP retrofitted reinforced concrete beam under bending, based on the concept of moment-curvature, is presented and it is applied to compute the complete nonlinear load-deflection curve, FRP-concrete interfacial shear stress, the FRP laminate strain and the debonding load of statically determinate RC beams retrofitted by an adhesively bonded FRP laminate. The beam may be subjected to any loading, including uniformly distributed or discrete point load(s). The governing equations satisfy the equilibrium and strain compatibility requirements of the beam but slip at the FRP-concrete interface is permitted. A novel procedure for constructing the full nonlinear moment-curvature relationship of beams undergoing interfacial slip is presented in detail, but it is shown that practically a trilinear relationship is satisfactory for obtaining an accurate estimate of the beam deflection and stresses. The robustness and accuracy of the method are demonstrated by analyzing several beams tested by other researchers under uniformly distributed load or four-point bending, with remarkably close agreement between the experimental and corresponding computed values.

Keywords: Analysis; Beam; Concrete; Curvature; Debonding; FRP; Modeling; Moment

1. Introduction

Repair and retrofit of damaged or deficient reinforced concrete (RC) members by fiber reinforced polymer (FRP) laminates, externally bonded by an adhesive to the concrete surface, is becoming a viable alternative to traditional repair techniques, such as steel plating or insertion of steel/FRP bars in grooves near the soffit of beams and slabs. The economic advantage and ease of application of this retrofit method is described by others [1]-[4]; however, its effectiveness depends on the ability of the adhesive and the concrete to resist the interfacial shear and normal stresses. The normal or peeling stress cannot be easily evaluated using experimental data, but some analytical methods have shown them to be relatively small [5] and current design standards/guidelines [6]-[10] ignore its presence; accordingly, in the current investigation it is disregarded.

Premature debonding of the FRP laminate from the concrete is often observed in the laboratory tests [11] primarily due to the inability of the concrete at its interface with the adhesive to resist the high shear stresses. The magnitude and distribution of these stresses depend on the type of loading acting

on the beam [12], the beam geometry, the steel reinforcement ratio, the concrete and steel reinforcement mechanical properties, the FRP laminate elastic modulus, strength and thickness as well as the adhesive mechanical properties. In the case of strong polymeric adhesives, such as epoxy, laboratory observations do not show failure within the adhesive, but the adhesive shear modulus and thickness do influence the debonding load [13]. From the structural safety point of view, knowledge of the debonding load is necessary, but in view of the dependency of the latter load on the interfacial shear stress and the many factors which influence the magnitude and distribution of that parameter, it is difficult to predict them accurately. Since debonding occurs in the concrete substrate and since concrete shear failure is brittle, it is difficult to justify the use of an average shear stress for predicting debonding.

Many studies have been made in the past to calculate the interfacial shear stresses using beam theory, theory of elasticity or finite element analysis [14]-[29].

In 1997, Taljsten [27] presented an analytical method of calculating the shear and normal stresses in the adhesive layer without considering the bending stiffness of the strengthened plate. The model is based on linear elastic theory and considers all the beam materials and interfaces to be behaving elastically. Although the method provides the concrete-FRP laminate interfacial shear stresses, it does not apply to concrete beams where the advent of concrete cracking and nonlinearity and steel yielding alter the interfacial stresses magnitude and distribution. Furthermore, the method does not deal with determination of the beam deflection and rotation, consequently, it cannot be used to determine these deformations. Following the Taljsten, Smith et Teng [28] proposed an analytical solution for evaluating the stresses in the adhesive layer for application to beams made of different materials and retrofitted by an adhesively bonded thin plate. Once again, material non-linearity was neglected and the solution is not applicable to reinforced concrete beams experiencing cracking and yielding. Rabinovitch [29] proposed an alternative approach for evaluating the interfacial stresses based on fracture mechanics. The approach involves evaluation of the energy release rate through the virtual crack extension method using various analytical and numerical stress analysis models, the assumption of linear elasticity for all the materials retained.

A mechanical model was proposed by Faella et al. [19] to simulate the behavior of RC beams strengthened by externally bonded FRP plates which accounted for the non-linear stress–strain relationships of concrete, steel and FRP-concrete interface. They assumed the RC beam to follow the Euler-Bernoulli beam theory and the FRP laminate was treated as conventional reinforcement, lacking flexural stiffness. The interaction between the laminate and the RC section was modelled via a continuous elastic interface layer with negligible thickness. They only compared the computed vertical deflection for a number of beams with the corresponding experimental values but made no attempt to compute the FRP strain or the interfacial stresses, which are often the quantities of interest in design of retrofitted concrete members. Finally, Attari et al. [20] evaluated the flexural capacity of reinforced concrete beams externally strengthened with FRP composites using conventional full strain compatibility and full bond between the FRP laminate and concrete up to failure, but these assumption do not conform to the real behavior of externally strengthened RC beams and studies of this type treat the laminate as another layer of reinforcement akin to the reinforcing steel in RC members.

Since reinforced concrete beams are typically strengthened to increase their ultimate strength and since at the ultimate state they experience cracking, concrete nonlinearity in compression and steel yielding, elastic analysis in this situation are not particularly useful because debonding generally occurs after the advent of cracking and yielding in the RC beam. The nonlinear finite element method

is theoretically able to solve this problem accurately, but it is time-consuming, expensive, require access to sophisticated computer software in the commercial domain and requires understanding and applying complex formulations, which is neither feasible nor justified in routine applications. Hence, there is a need for a simple, yet accurate and robust method of analysis such as the one presented in the current investigation. Although some previous simplified analytical solutions [30]-[31] have considered non-linearity of concrete material, they only provide the retrofitted beam mid-span deformations and apply an iterative approach to satisfy full strain compatibility and equilibrium, but they neglect the presence of slip at the laminate-concrete interface. Finally, to our knowledge all the previous solutions have assumed beams under four point bending, but in practical applications beams are designed to commonly carry uniformly distributed dead and live loads. Thus, the existing analytical solutions as currently presented, other than those based on the full bond assumption, cannot be applied to beams under uniform load.

The proposed formulation accounts for the changes in the beam stiffness and interfacial properties under increasing load by dividing the beam along its length into several regions and by enforcing the compatibility and equilibrium requirements at the points where the regions meet. Such solutions do not represent accurately the laminate-concrete interfacial behavior due to the assumption of full bond and are unable to accurately predict laminate debonding.

In view of the above comments, a new formulation, based on the concept of moment-curvature relationship, is developed. The formulation uses more refined constitutive laws for concrete in tension and compression and a bilinear elastic-slip softening interfacial shear-slip law. The computed curvature at any section is expressed in terms of the level of slip at that section, which allows one to solve the second order governing equations of the beam while fully satisfying the equilibrium requirements. To simplify the solution and make the method more appealing for practical applications, the actual nonlinear moment-curvature relationship is idealized by a trilinear curve to represent the uncracked, crack-unyielded and cracked-yielded states of the RC section. As will be seen later, notwithstanding this simplification, the predictions of the model agree remarkably well with available experimental data from beams tested in four-point bending or uniformly distributed load.

2. Analytical formulation

Let Fig. 1 represent half of a symmetrical RC beam retrofitted with an FRP laminate adhesively bonded to its tension face and subjected to uniformly distributed load q. Note, the proposed methodology is not theoretically restricted to symmetrically or uniformly loaded, but these are imposed to make the presentation simpler.

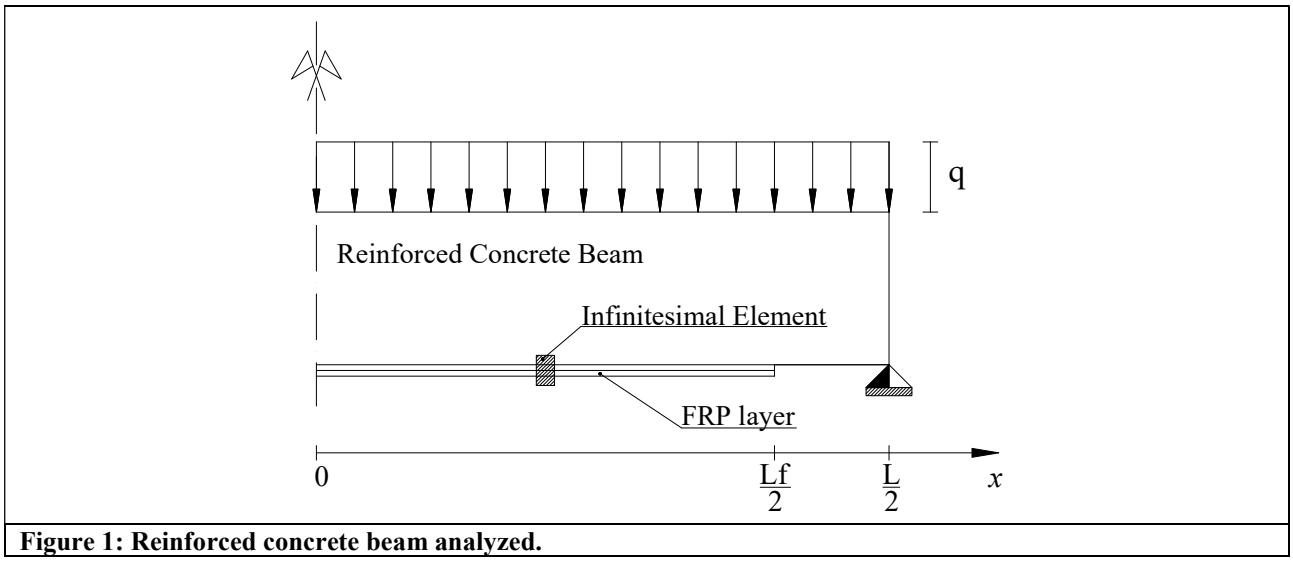

Figure 1: Reinforced concrete beam analyzed.

A typical cross-section of the retrofitted beam, subjected to an external moment, is depicted in Fig. 2. Observe that F_c, and M_c are the force and moment resultants of the stresses in the concrete and internal steel reinforcement acting through the centroid of the concrete section. To satisfy equilibrium, F_c must equal F_f, the tensile force resisted by the FRP laminate.

Let the centroidal axial displacement of the concrete section, the tensile steel and the FRP be u_c, u_s, and u_f, respectively. Then, the slip λ at the concrete-FRP interface can be expressed as

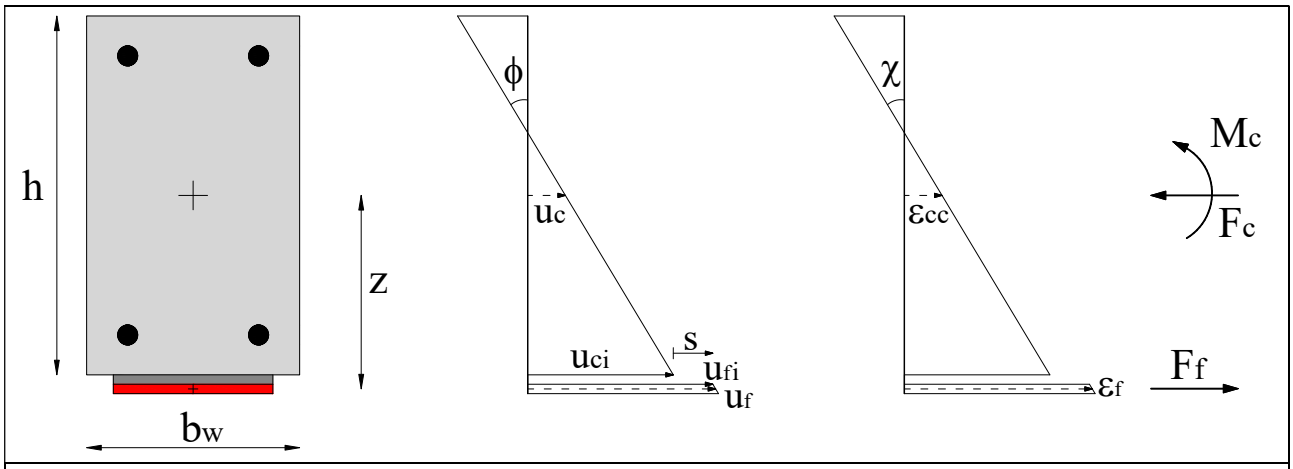

Figure 2: Transverse section of FRP-strengthened RC beam.

$$\lambda = u_{ci} - u_{fi} = u_c - u_f + \phi z \qquad (1)$$

where u_{ci} and u_{fi}, respectively, represent the axial displacement of the concrete and FRP at their interface, ϕ is the section rotation and z is the distance between the centroids of the concrete section and the FRP laminate. It is important to point out that in the presents model the concrete section and the FRP laminate are assumed to have equal vertical displacement and rotation at any section. The calculation of slip per Eq. 1 is similar to the one used by previous researchers [27].

Considering the moment equilibrium of the retrofitted section,

$M_e = M_c + M_f$	(2a)
$M_c = C_s d'_s + T_c \overline{d}_c + T_s \overline{d}_s$	(2b)
$M_f = T_f d_f$	(2c)

and

$F_c = C_c + C_s - T_c - T_s$	(3a)
$F_f = T_f$	(3b)

From equilibrium of internal axial forces

$F_c = T_f$	(4)

where M_e is the external moment acting on the section, M_c is the moment of the forces acting on the concrete section in the retrofitted beam and M_f is the moment of the force in the FRP, with moments taken about the axis coincident with the line of action of the resultant compressive force, C_c, in the concrete. All the moment arms, $d'_s, \overline{d}_c, \overline{d}_s, d_f$ in Eq. 2(b) and (c) are measured from the preceding moment axis. In the above equations, C_s, T_c, and T_s are the resultant forces resisted by the compressive steel, the concrete under tension and the tensile steel reinforcement, respectively.

From equilibrium of the horizontal forces acting on the infinitesimal FRP element in Fig. 1, the interfacial shear flow is given by

$\frac{dF_f}{dx} = -\tau b_f$	(5)

where b_f is the laminate width and τ is the interfacial shear stress. Notice, in the current formulation the origin of the coordinate x is located at midspan. The interfacial shear is a function of the slip λ at the FRP laminate-concrete interface, or more precisely adhesive-concrete interface. The shear-slip law adopted in this study is shown in Fig. 3.

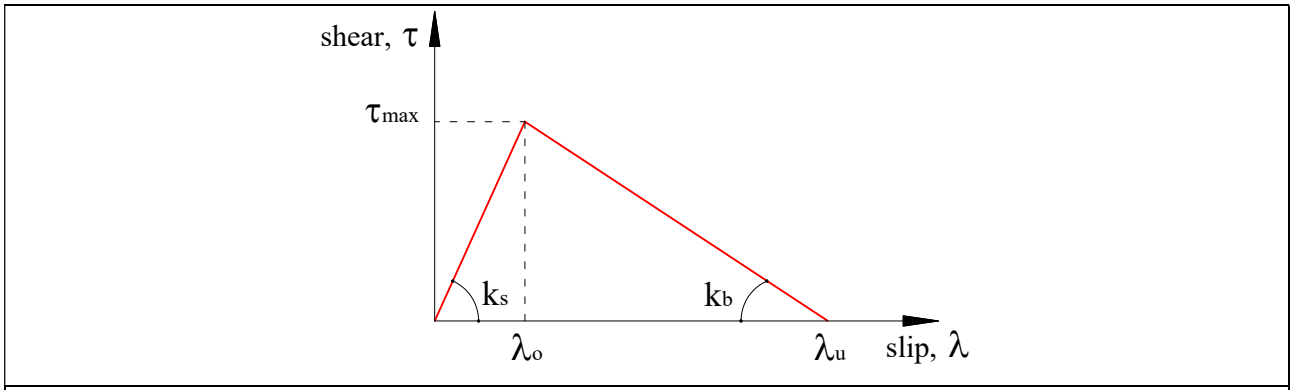

Figure 3: FRP-concrete interfacial shear slip law.

This law was shown by Ascione [32], Ascione et al. [33], and Cosenza et al. [34] to give satisfactory results when compared to experimental data. It is an empirical law, thus theoretically the values of

$\tau_{\max}, \lambda_o$ and λ_u must be defined by the user, but as shown in the latter three references, in the absence of specific data, sufficient experimental data exists to guide the user in selecting reasonable values. The choice of the shear slip law does not affect the fundamental analytical procedure developed here, but it may affect the results in the same way as values of concrete and FRP strength and elastic moduli are expected to affect them. The precise choice of this law is beyond the scope of this paper, but reference can be made to Ascione et al. [33] for further insight.

The moment M_c can be related to the section curvature χ. It is relatively straightforward to construct the full moment-curvature relationship of any concrete section under the assumption of full bond between the concrete and the reinforcement, but when slip can occur, as in the current problem, an alternative procedure is required. The procedure used here is presented in full in Appendix A of this paper, but for now let us approximate the $M_c - \chi$ response as a trilinear curve as shown in Fig. 4(a). Notice in the latter figure that the idealized trilinear curve closely approximates the actual fully nonlinear curve. In the figure, the moments M_{cr}, M_y and M_u, respectively, represent the retrofitted section cracking, yielding and ultimate moment while χ_{cr}, χ_y and χ_u, denote the corresponding curvatures.

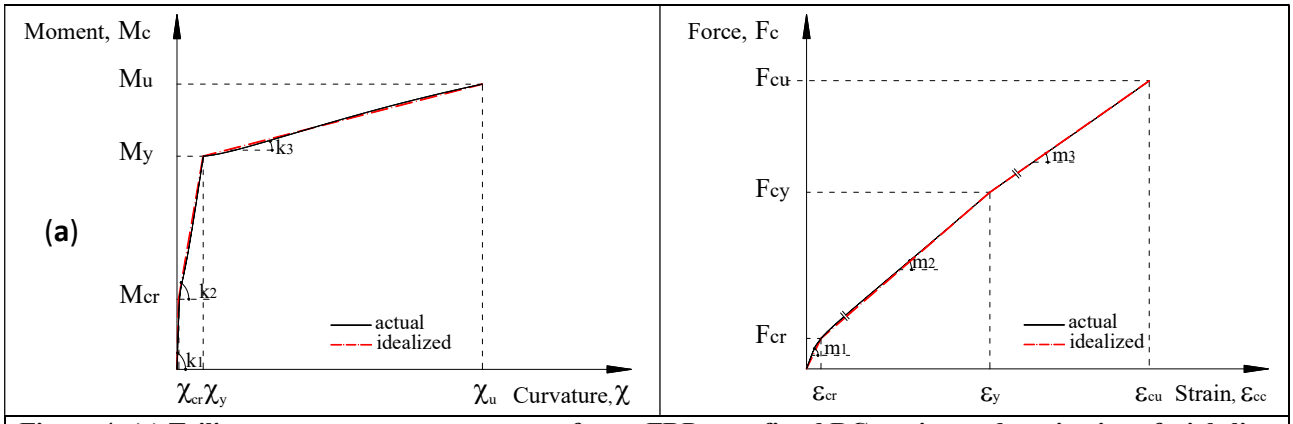

Figure 4: (a) Trilinear moment-curvature curve for an FRP retrofitted RC section undergoing interfacial slip. (b) Trilinear RC section resultant compression force-extreme bottom fiber strain curve.

The slope of the three linear segment of the idealized curve are denoted by k_1, k_2 and k_3, which represent the flexural rigidity of the three commonly observed states of the cross-section (uncracked, cracked-unyielded and cracked-yielded) henceforth, designated as State 1, 2 and 3, respectively. The trilinear curve more accurately represents the behavior of RC sections than the bilinear curve previously used by Mostafa and Razaqpur [5] or the elastic-perfectly plastic relationship commonly used in other analytical solutions [18]. With reference to Fig. 4(a), for the above states, one can write

$M_c = k_1 \chi$ for $\chi \le \chi_{cr}$	(6a)
$M_c = M_{cr} + k_2 (\chi - \chi_{cr})$ for $\chi_{cr} < \chi \le \chi_y$	(6b)
$M_c = M_y + k_3 (\chi - \chi_y)$ for $\chi_y < \chi \le \chi_u$	(6c)

By satisfying the slip condition (Eq. 1) and equilibrium (Eq. 2-3) requirements, and by using the interface shear-slip relationship (Eq. 5) and the constitutive relations (Eq. 6), the solution of the

governing equations can be obtained, depending on the evolution of interfacial slip and the state of the RC section as explained below.

(i) *For Slip Level I:* $\lambda \le \lambda_o$

Since slip is independent of the state of the cross-section, at any slip level, the RC section could be in any of the above-mentioned states. The governing equation can be solved for each state, subject to the $\lambda \le \lambda_o$ constraint as shown below.

Considering Eq. (1) and the shear-slip relationship in Fig. 3, the rotation of the RC section, ϕ, can be expressed as:

$$\phi = \left(u_f - u_c - \frac{t_f E_f}{k_s} \varepsilon_f' \right) \frac{1}{d} \tag{7}$$

where E_f and ε_f are the elastic modulus and axial strain of the FRP laminate, respectively.

In view of Eq. (7), the curvature, χ, is given by

$$\chi = \frac{d\phi}{dx} = \left(\varepsilon_f - \varepsilon_c - \frac{t_f E_f}{k_s} \varepsilon_f'' \right) \frac{1}{d} \tag{8}$$

The external moment, M_e, due to the applied load acting on the retrofitted RC beam, is equilibrated at any section by the sum of the resisting moment of the un-retrofitted RC section, M_c, and the resisting moment of the FRP, M_f, where

$$M_f = T_f d_f = b_f t_f E_f \varepsilon_f d_f \tag{9}$$

Note, for a given extreme concrete fiber strain in an RC section, the M_c of the retrofitted section is not the same as that of the un-retrofitted section; hence, M_c cannot be determined by using the moment-curvature relationship of the un-retrofitted section.

Considering Eqs. (5), (8), (9) and the moment-curvature relation in Fig.4(a), after some algebraic manipulations, for slip level I, Eqs (10a), (10b) and (10c), can be derived, corresponding to State 1, 2 and 3, respectively.

$$\chi'' - \omega_{I,1}^2 \chi = \frac{1}{k_1} \frac{d^2 M_e}{dx^2} - \frac{\omega_{I,1}^2}{b_{I,1}^2} M_e \tag{10a}$$

$$\chi'' - \omega_{I,2}^2 \chi = \frac{1}{k_2} \frac{d^2 M_e}{dx^2} - \frac{\omega_{I,2}^2}{b_{I,2}^2} \left(M_e - M_{cr} + k_2 \chi_{cr} \right) \tag{10b}$$

$$\chi'' - \omega_{I,3}^2 \chi = \frac{1}{k_3} \frac{d^2 M_e}{dx^2} - \frac{\omega_{I,3}^2}{b_{I,3}^2} \left(M_e - M_y + k_3 \chi_y \right) \tag{10c}$$

(ii) *For Slip Level II:* $\lambda_o < \lambda \le \lambda_u$

For slip level II, an equation similar to Eq. (7) can be written as

$$\phi = \left(\lambda_u + u_f - u_c + \frac{t_f E_f}{k_b} \varepsilon'_f \right) \frac{1}{d} \tag{11}$$

Differentiating Eq. (11) gives the curvature at slip level II as

$$\chi = \left(\varepsilon_f - \varepsilon_c + \frac{t_f E_f}{k_b} \varepsilon''_f \right) \frac{1}{d} \tag{12}$$

Finally, as in the case of slip level I, for slip level II, Eq. (13a) to (13c), can be written for State 1 to 3 of the section, respectively

$$\chi'' + \omega_{II,1}^2 \chi = \frac{1}{k_1} \frac{d^2 M_e}{dx^2} + \frac{\omega_{II,1}^2}{b_{II,1}^2} M_e \tag{13a}$$

$$\chi'' + \omega_{II,2}^2 \chi = \frac{1}{k_2} \frac{d^2 M_e}{dx^2} + \frac{\omega_{II,2}^2}{b_{II,2}^2} \left(M_e - M_{cr} + k_2 \chi_{cr} \right) \tag{13b}$$

$$\chi'' + \omega_{II,3}^2 \chi = \frac{1}{k_3} \frac{d^2 M_e}{dx^2} + \frac{\omega_{II,3}^2}{b_{II,3}^2} \left(M_e - M_y + k_3 \chi_y \right) \tag{13c}$$

In Eqs. (10) and (13), the symbols $\omega_{i,j}^2 = a_{i,j}^2 b_{i,j}^2 \, (i = I, II; j = 1,2,3)$ denote the following:

$$\omega_{I,1}^2 = \frac{k_s b_f}{k_1 m_1^*} \left(k_1 + m_1^* \overline{d}_f^2 \right) = a_{I,1}^2 \left(b_{I,1}^2 \right) \tag{14a}$$

$$\omega_{I,2}^2 = \frac{k_s b_f}{k_2 m_2^*} \left(k_1 + m_2^* \overline{d}_f^2 \right) = a_{I,2}^2 \left(b_{I,2}^2 \right) \tag{14b}$$

$$\omega_{I,3}^2 = \frac{k_s b_f}{k_3 m_3^*} \left(k_3 + m_3^* \overline{d}_f^2 \right) = a_{I,3}^2 \left(b_{I,3}^2 \right) \tag{14c}$$

$$\omega_{II,1}^2 = \frac{k_b b_f}{k_1 m_1^*} \left(k_1 + m_1^* \overline{d_f}^2 \right) = a_{II,1}^2 \left(b_{II,1}^2 \right) \tag{14d}$$

$$\omega_{II,2}^2 = \frac{k_b b_f}{k_2 m_2^*} \left(k_2 + m_2^* \overline{d_f}^2 \right) = a_{II,2}^2 \left(b_{II,2}^2 \right) \tag{14e}$$

$$\omega_{II,3}^2 = \frac{k_b b_f}{k_3 m_3^*} \left(k_3 + m_3^* \overline{d_f}^2 \right) = a_{II,3}^2 \left(b_{II,3}^2 \right) \tag{14f}$$

where m_i^* (i =1,2,3) is equal to :

$$m_i^* = \frac{m_i A_f E_f}{m_i - A_f E_f} \tag{15}$$

where m_i (i =1,2,3) is the slope of segment i in the idealized trilinear F_c-ε_{cc} diagram illustrated in Fig. 4(b).

The method for the construction of the latter diagram is described in Appendix A.

The beam rotation $\phi(x)$ and vertical displacement $v(x)$ at any section along its length is computed by integration of the beam curvature along its length, i.e.

$$\phi(x) = \int \chi(x) dx \tag{16a}$$

$$v(x) = \iint \chi(x) dx \tag{16b}$$

3. Solution of the governing equations and calculation of stresses and displacements

3.1 Solution method

The solutions of the second order governing differential equations Eqs. (10a) to (10c), corresponding to slip level I and section State 1,2 and 3, respectively, are given by Eqs. (17a) to (17c), respectively

$$\chi(x) = A_{I,1} e^{\omega_{I,1} x} + B_{I,1} e^{-\omega_{I,1} x} + \frac{1}{\omega_{I,1}^2 k_1}\left(a_{I,1}^2 k_1 M_e - \frac{d^2 M_e}{dx^2} \right) \tag{17a}$$

$$\chi(x) = A_{I,2} e^{\omega_{I,2} x} + B_{I,2} e^{-\omega_{I,2} x} + \frac{1}{\omega_{I,2}^2 k_2}\left[a_{I,2}^2 k_2 \left(M_e - M_{cr} + \chi_{cr} k_2 \right) - \frac{d^2 M_e}{dx^2} \right] \tag{17b}$$

$$\chi(x) = A_{I,3} e^{\omega_{I,3} x} + B_{I,3} e^{-\omega_{I,3} x} + \frac{1}{\omega_{I,3}^2 k_3}\left[a_{I,3}^2 k_3 \left(M_e - M_y + \chi_y k_3 \right) - \frac{d^2 M_e}{dx^2} \right] \tag{17c}$$

The solutions of Eqs. (13a) to (13c), corresponding to slip level II and section State 1,2 and 3, respectively, are given by Eqs. (18a) to (18c), respectively

$$\chi(x) = A_{II,1} \sin\left(\omega_{II,1} x\right) + B_{II,1} \cos\left(\omega_{II,1} x\right) + \omega_{II,1}^2 k_1 \left[a_{II,1}^2 k_1 \left(M_e \right) + \frac{d^2 M_e}{dx^2} \right] \tag{18a}$$

$$\chi(x) = A_{II,2} \sin\left(\omega_{II,2} x\right) + B_{II,2} \cos\left(\omega_{II,2} x\right) + \omega_{II,2}^2 k_2 \left[a_{II,2}^2 k_2 \left(M_e - M_{cr} + \chi_{cr} k_2 \right) + \frac{d^2 M_e}{dx^2} \right] \tag{18b}$$

$$\chi(x) = A_{II,3} \sin\left(\omega_{II,3} x\right) + B_{II,3} \cos\left(\omega_{II,3} x\right) + \omega_{II,3}^2 k_3 \left[a_{II,3}^2 k_3 \left(M_e - M_y + \chi_y k_3 \right) + \frac{d^2 M_e}{dx^2} \right] \tag{18c}$$

The integration constants $A_{i,j}$ and $B_{i,j}$ in each case can be evaluated based on the boundary conditions of the beam. For a symmetrically loaded simply supported beam,

$$\chi\left(\frac{L}{2}\right) = 0 \tag{19a}$$

$\chi'(0)=0$	(19b)

Note $\frac{d^2M_e}{dx^2}=-q(x)$, where *q(x)* is the applied distributed load acting on the beam, which is zero in the case of applied concentrated loads. In the case of a uniformly loaded beam,

$M_e=\frac{q}{2}\left(\frac{L^2}{4}-x^2\right)$	(20)

3.2 Determination of FRP laminate strain and stress

Once the relevant curvature is determined, the FRP strain, ε_f, at any section is given by

$\varepsilon_f=\left(h+\frac{t_f}{2}-c\right)\chi$	(21)
$\sigma_f=E_f\varepsilon_f$	(22)

where *h* is the RC section height, t_f the thickness of the laminate and *c* is the depth of the neutral axis. Both c and χ depend on the level of the applied load.

3.3 Beam deflection calculation

As stated earlier, the beam rotation and deflection can be determined using Eqs. 16(a) and (b). However, the correct expression for the curvature must be selected, depending on the interfacial slip level and the stress state of the RC section. At points along the beam where there is abrupt change in the beam stress state, one must choose the appropriate curvature expressions for the segments to the right and left of the transition point while concurrently satisfying the equality of displacement and rotation of the two segments at the same point. Therefore, inserting for curvature from Eqs. 12 and 13 into Eq. 16(b) leads to the following three equations for the deflected shape of the beam.

(i) Beam deflection equations for slip level I and section States 1,2 and 3, respectively:

$v(x)=\frac{1}{\omega_{I,1}^2}\left(A_{I,1}e^{\omega_{I,1}x}+B_{I,1}e^{-\omega_{I,1}x}\right)+C_{I,1}x+D_{I,1}+\frac{1}{2\omega_{I,1}^2k_1}\left[2a_{I,1}^2k_1\iint\left(M_e-\frac{d^2M_e}{dx^2}\right)dx^2\right]$	(23a)

$$v(x)=\frac{1}{\omega_{I,2}^2}\left(A_{I,2}e^{\omega_{I,2}x}+B_{I,2}e^{-\omega_{I,2}x}\right)+C_{I,2}x+D_{I,2}+\ldots$$ $$\ldots+\frac{1}{2\omega_{I,2}^2k_2}\left\{a_{I,2}^2k_2\left[2\iint\left(M_e-\frac{d^2M_e}{dx^2}\right)dx^2+\left(\chi_{cr}k_2-M_{cr}\right)x^2\right]\right\}$$	(23b)
$$v(x)=\frac{1}{\omega_{I,3}^2}\left(A_{I,3}e^{\omega_{I,3}x}+B_{I,3}e^{-\omega_{I,3}x}\right)+C_{I,3}x+D_{I,3}+\ldots$$ $$\ldots+\frac{1}{2\omega_{I,3}^2k_3}\left\{a_{I,3}^2k_3\left[2\iint\left(M_e-\frac{d^2M_e}{dx^2}\right)-dx^2+\left(\chi_yk_3-M_{cy}\right)x^2\right]\right\}$$	(23c)

Similarly,

(ii) Beam deflection equations for slip level II and section States 1, 2, and 3, respectively:

$$v(x)=\frac{1}{\omega_{II,1}^2}\left[A_{II,1}\sin\left(\omega_{II,1}^2x\right)+B_{II,1}\cos\left(\omega_{II,1}^2x\right)\right]+C_{II,1}x+D_{II,1}+\ldots$$ $$\ldots+\frac{1}{2\omega_{II,1}^2k_1}\left\{a_{II,1}^2k_1\left[2\iint\left(M_e+\frac{d^2M_e}{dx^2}\right)dx^2\right]\right\}$$	(24a)
$$v(x)=\frac{1}{\omega_{II,2}^2}\left[A_{II,2}\sin\left(\omega_{II,2}^2x\right)+B_{II,2}\cos\left(\omega_{II,2}^2x\right)\right]+C_{II,2}x+D_{II,2}+\ldots$$ $$\ldots+\frac{1}{2\omega_{II,2}^2k_2}\left\{a_{II,2}^2k_2\left[2\iint\left(M_e+\frac{d^2M_e}{dx^2}\right)dx^2+\left(\chi_{cr}k_2-M_{cr}\right)x^2\right]\right\}$$	(24b)
$$v(x)=\frac{1}{\omega_{II,3}^2}\left[A_{II,3}\sin\left(\omega_{II,3}^2x\right)+B_{II,3}\cos\left(\omega_{II,3}^2x\right)\right]+C_{II,3}x+D_{II,3}+\ldots$$ $$\ldots+\frac{1}{2\omega_{II,3}^2k_3}\left\{a_{II,3}^2k_3\left[2\iint\left(M_e+\frac{d^2M_e}{dx^2}\right)dx^2+\left(\chi_yk_3-M_{cy}\right)x^2\right]\right\}$$	(24c)

It is important to emphasize that Eq. (23a) only applies to segments along the beam with slip level I and stress state 1, (23b) to segments with slip level I and stress state 2 and (23c) to segments with slip level I and stress state 3. For slip level II the corresponding equations are Eqs. (24a) to (24c).

The constants $C_{i,j}$ and $D_{i,j}$ (i = *I,II;* j=*1,2,3*) are determined by applying the following boundary conditions:

$$v\left(\frac{L}{2}\right)=0$$	(25a)

$v'(0)=0$	(25b)

Additional constraints are imposed on the solution to ensure equality of displacement and rotation of the beam at the neighboring segments common points. These constraints, together with the latter boundary conditions, provide sufficient equations to solve for the unknown coefficients.

4. Numerical solution scheme

The beam is divided into several finite segments and since the problem is nonlinear, the load is applied incrementally. Initially, all the segments will be uncracked (State 1) and will have zero slip (slip level I), thus the solution would be based on linear elasticity. Hence, the first load increment could correspond to the beam cracking moment, provided slip level I is not exceeded. Once a segment is cracked, its stress state will change. Therefore, depending on its slip level and stress state, the appropriate beam flexural rigidity, curvature and deflection equation need to be applied. At the common point of adjoining segments x_i and x_{i+1}, the following continuity conditions must be satisfied:

$\chi_{i,j}(x_i)=\chi_{i,j}(x_{i+1})$ (continuity of curvature)	(26a)
$\frac{d\chi_{i,j}(x_i)}{dx}=\frac{d\chi_{i,j}(x_{i+1})}{dx}$ (continuity of strain)	(26b)

and

$v_{i,j}(x_i)=v_{i,j}(x_{i+1})$ (continuity of vertical displacement)	(27a)
$\frac{dv_{i,j}(x_i)}{dx}=\frac{dv_{i,j}(x_{i+1})}{dx}$ (continuity of rotation)	(27b)

Due to the nonlinear nature of the problem, the solution must be iteratively performed, and the iteration will be terminated once a pre-selected convergence criterion is satisfied. In the present analysis, at the common point of each two adjoining segments, the shear stress is calculated after each iteration and if the difference between two consecutive iterations, $\Delta\tau$, is less than or equal to a preset convergence tolerance ρ, as indicated in Eq. (28), iteration is terminated and the new load increment is applied. Also, at the transition points of the beam from one stress state to another, it is checked to make sure the moment corresponds to either M_{cr} (at transition from State 1 to 2) or M_y (at transition from State 2 to 3).

$\lvert\Delta\tau\rvert\le\rho$	(28)

5. Validation of the theoretical model

To assess the robustness and accuracy of the proposed model, several FRP retrofitted RC beams, which have been previously tested by others, are analyzed. All the beams are simply supported,

retrofitted with CFRP laminate and subjected to either simulated uniformly distributed load or four-point bending. The detailed properties of the beams are presented in Table 1. As the values of certain parameters in the tests were not reported, values are assumed for them in the current calculations, and the assumed values are shown in italics in Table 1. These values are chosen based on known values in the literature for similar parameters.

The beams were tested in the laboratory by Mazzotti and Savoia [35], Pan et al. [12], Fu et al. [36] Mostafa and Razaqpur [5], Maalej and Leong [37] and Spyrakos et al. [38]. For convenience, in Table 1, the beams in these studies are designated as Case (a), (b), (c), (d), (e) and (f), respectively. The beams in Case (a) to (c) had rectangular cross-section while in Case (d) it had a T-section. As may be observed in the Table 1, in some of these investigations, more than one beam was tested (Case (d)).

1 **Table 1. Geometrical and material properties of RC retrofitted beams analyzed**

Property	Unit	Beam					
		Case (a) [35]	Case (b) [12]	Case (c) [36]	Case (d) [5]	Case (e) [37]	Case (f) [38]
Flange thickness, t	mm	-	-	-	100	-	-
Beam height, h	mm	400	200	450	400	292	500
Web width, b_w	mm	250	150	200	250	230	250
Flange width, b_F	mm	-	-	-	500	-	-
Reinforcement cover	mm	30	*30*	37	40	30	20
Tension steel area, A_s	mm^2	462	157	402	530	942	307
Compression steel area, A_s'	mm^2	226	-	402	157	628	307
Beam span length, L	mm	3000	1800	4000	4500	3000	4500
Shear span, a	mm	-	-	-	1320	1000	-
		-	-	-	-	-	-
FRP laminate width, b_f	mm	250	450	100	220	215.6	200
FRP laminate length, L_f	mm	2900	1650	3800	4100	2900	4500
FRP laminate thickness, t_f	mm	0.260	0.220	0.990	0.165	0.330	0.510
Concrete strength, f_c'	MPa	47.90	59.00	48.50	54.00	39.8	20
Concrete ultimate strain, ε_{cu}	-	*0.035*	*0.035*	0.035	0.035	*0.0035*	*0.0035*
Concrete elastic modulus, E_c	GPa	37	39	37	37	33	28
Concrete cracking strain, ε_t	-	0.00015	0.00015	0.00015	0.00016	0.00013	0.00010
Concrete tensile strength, f_t	MPa	4.01	4.15	4.02	4.30	3.18	2.00
Concrete curve-fitting factor, *n*	-	*2*(1)	*2*	*2*	*2*	*2*	*2*
Concrete curve-fitting factor, *k*	-	*1*	*1*	*1*	*1*	*1*	*1*
Steel elastic modulus, E_s	GPa	*202*	202	187	192	183	200
Steel yield stress, f_y	MPa	550	550	431	407	544	500
Steel yield strain, ε_y	-	*0.0024*	0.0027	*0.0024*	0.0024	0.0035	*0.0025*
Steel strain corresponding to its ultimate strength, ε_{su}	-	*0.075*	*0.090*	*0.070*	0.090	*0.010*	*0.070*
FRP elastic modulus, E_f	GPa	290	235	258	227	235	240
FRP ultimate strain, ε_{fu}	-	0.014	0.018	0.018	0.0167	0.015	0.015
Maximum shear stress, τ_{max}	MPa	*3.00*	*3.00*	*3.00*	*3.00*	*3.00*	*3.00*
Slip corresponding to τ_{max}, λ_0	mm	*0.05*	*0.05*	*0.05*	*0.05*	*0.05*	*0.05*
Ultimate slip, λ_u	mm	*0.40*	*0.40*	*0.40*	*0.40*	*0.40*	*0.40*

2 (1) Values in italics are assumed due to lack of reported values in the tests

Figures 5 and 6 show for the beam TN5. tested in Case (a), the computed and experimentally measured mid-span moment-curvature relationship and the FRP laminate strain distribution along its length, respectively,

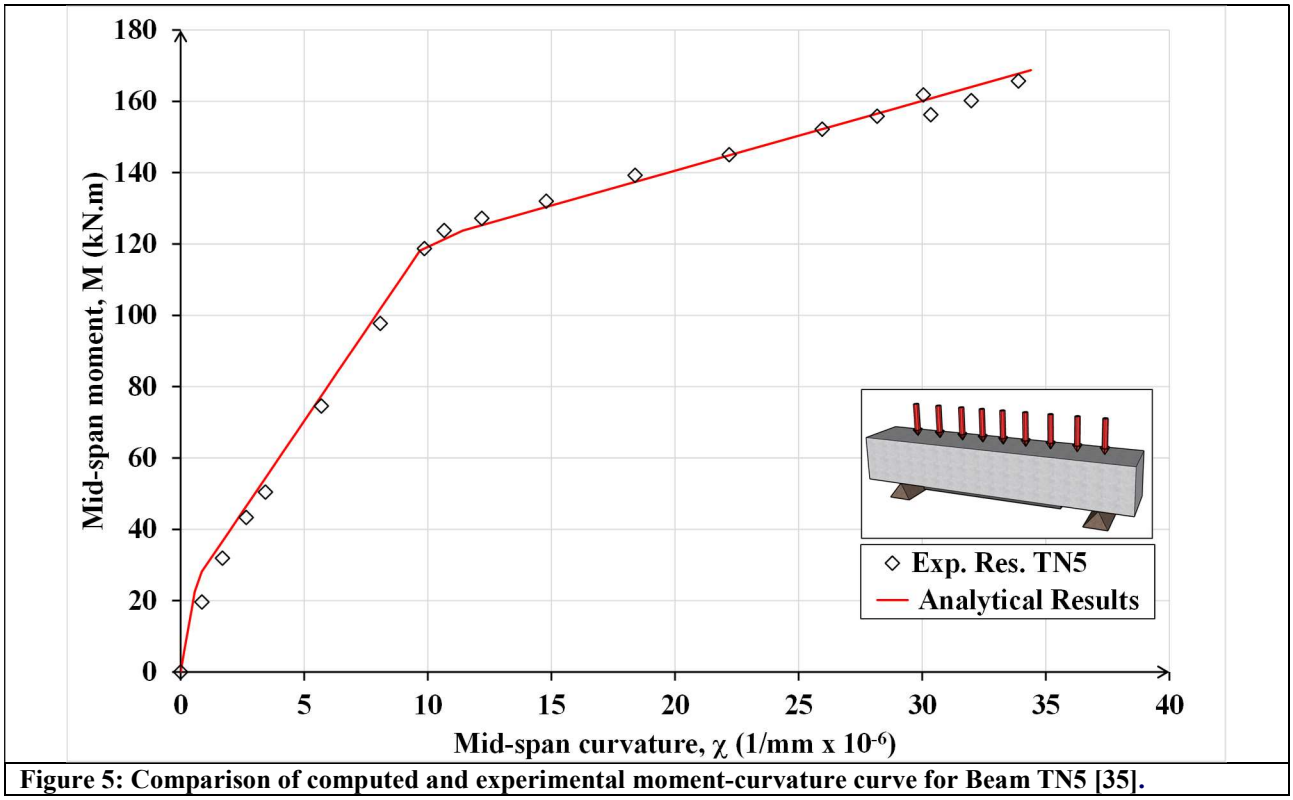

Figure 5: Comparison of computed and experimental moment-curvature curve for Beam TN5 [35].

The FRP strain is plotted for two load levels, one before the tension steel yielding (M_m = 100 kN.m) and the other after yielding (M_m = 150 kN.m), where M_m is the maximum moment acting on the beam.

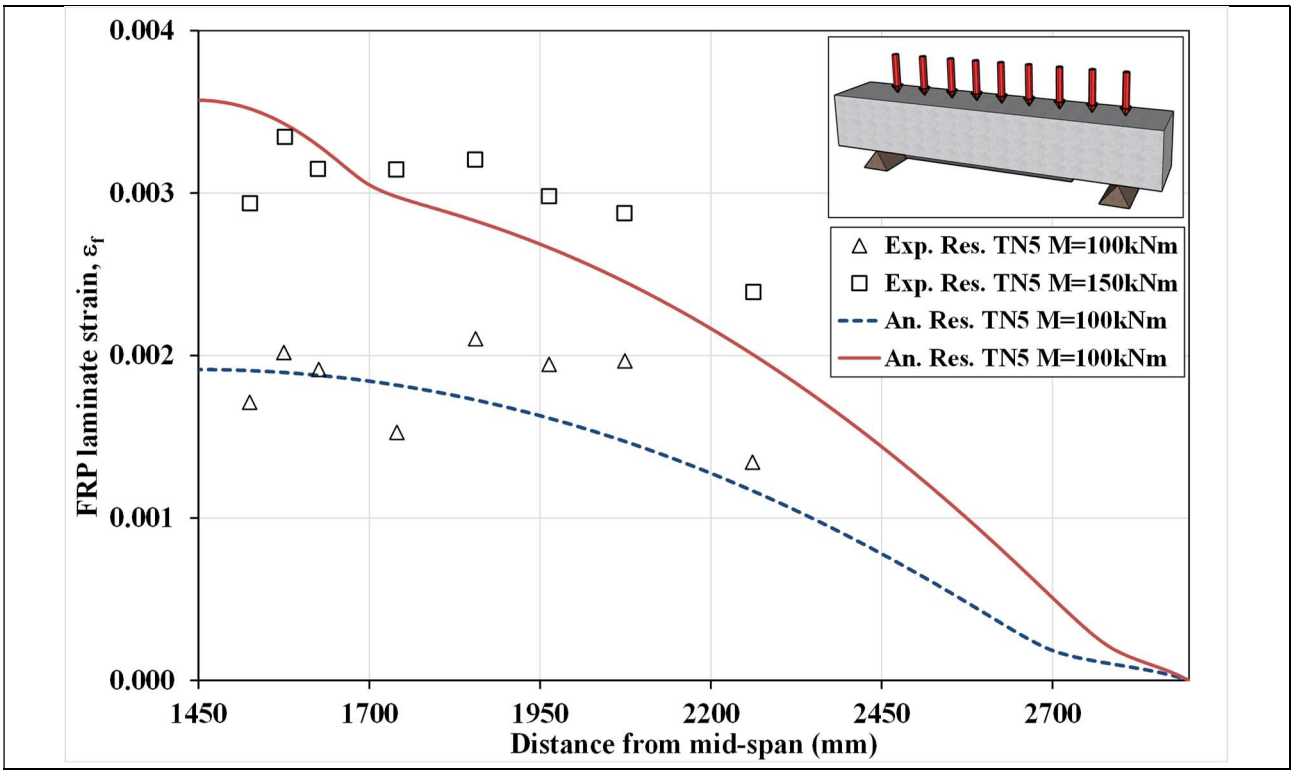

Figure 6. Comparison of computed and measured FRP strain variation in Beam TN5 in Case(a) at two load levels [35].

Figures 7 and 8 show the computed and corresponding experimentally measured mid-span moment-displacement curves for the uniformly loaded beams tested in Case (b) and (c), respectively. Notice, in Case (c) duplicate beams were tested and are designated as LP4 and LP8.

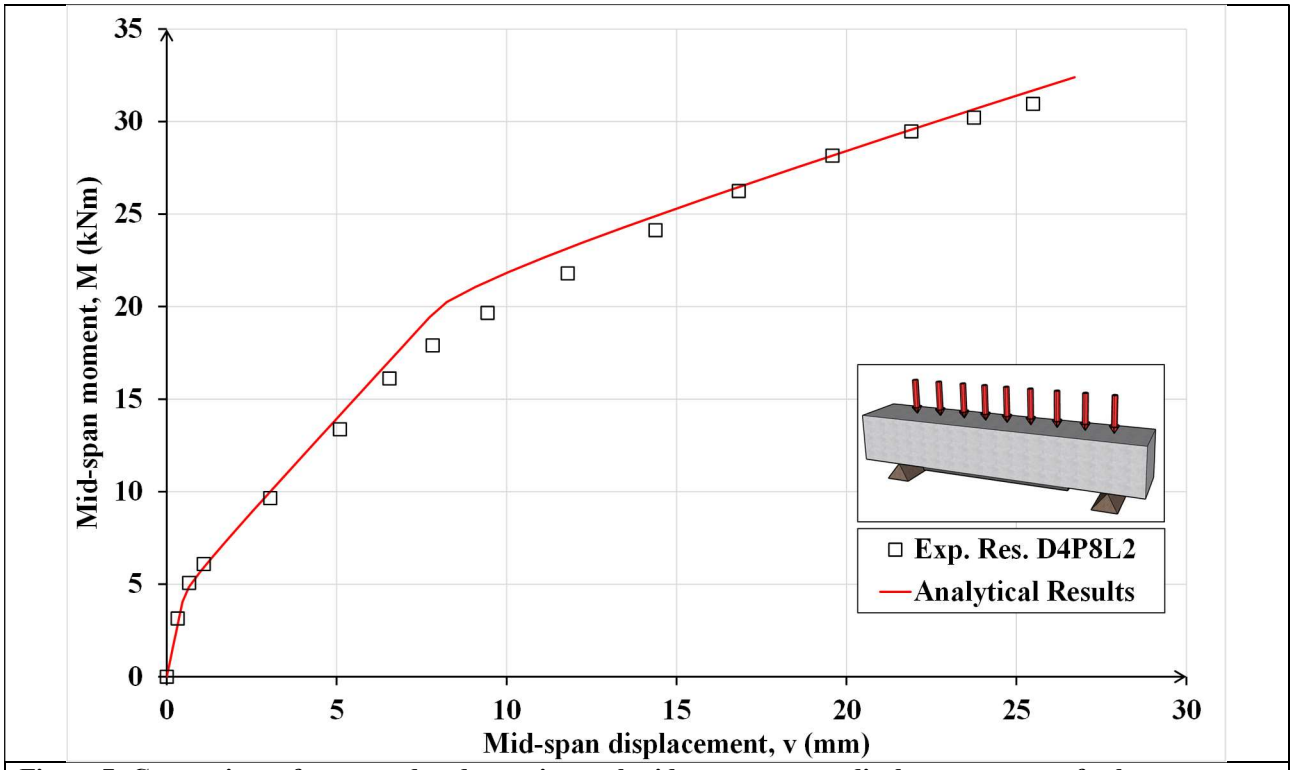

Figure 7: Comparison of computed and experimental mid-span moment-displacement curve for beam D4P8L2 in Case (b) [12].

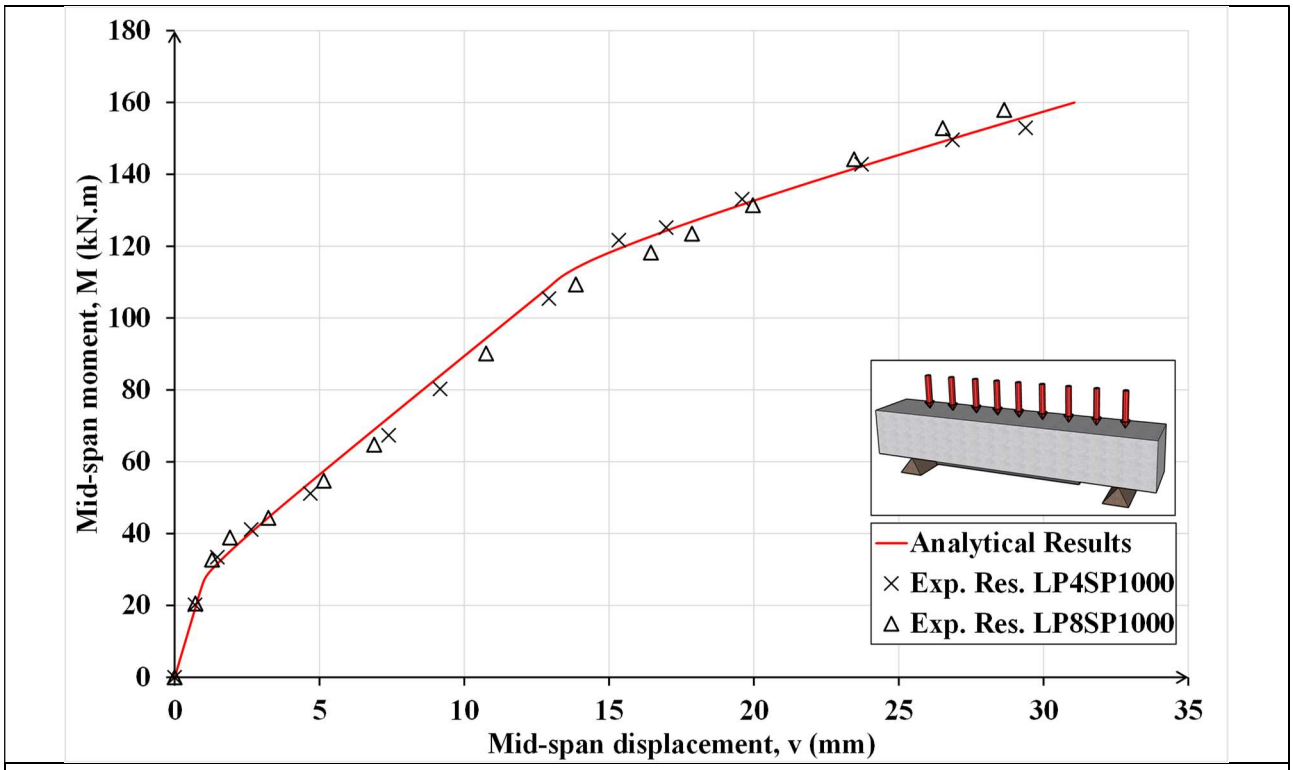

Figure 8: Comparison of computed and experimental mid-span moment-displacement curves for beams LP4 and LP8 in Case (c) [36].

Fig. 9 shows for the uniformly loaded rectangular beam in Case (c), designated as LP8, the CFRP laminate strain distribution along its length under a maximum moment of 156.7 kN.m, which is practically equal to the beam failure moment.

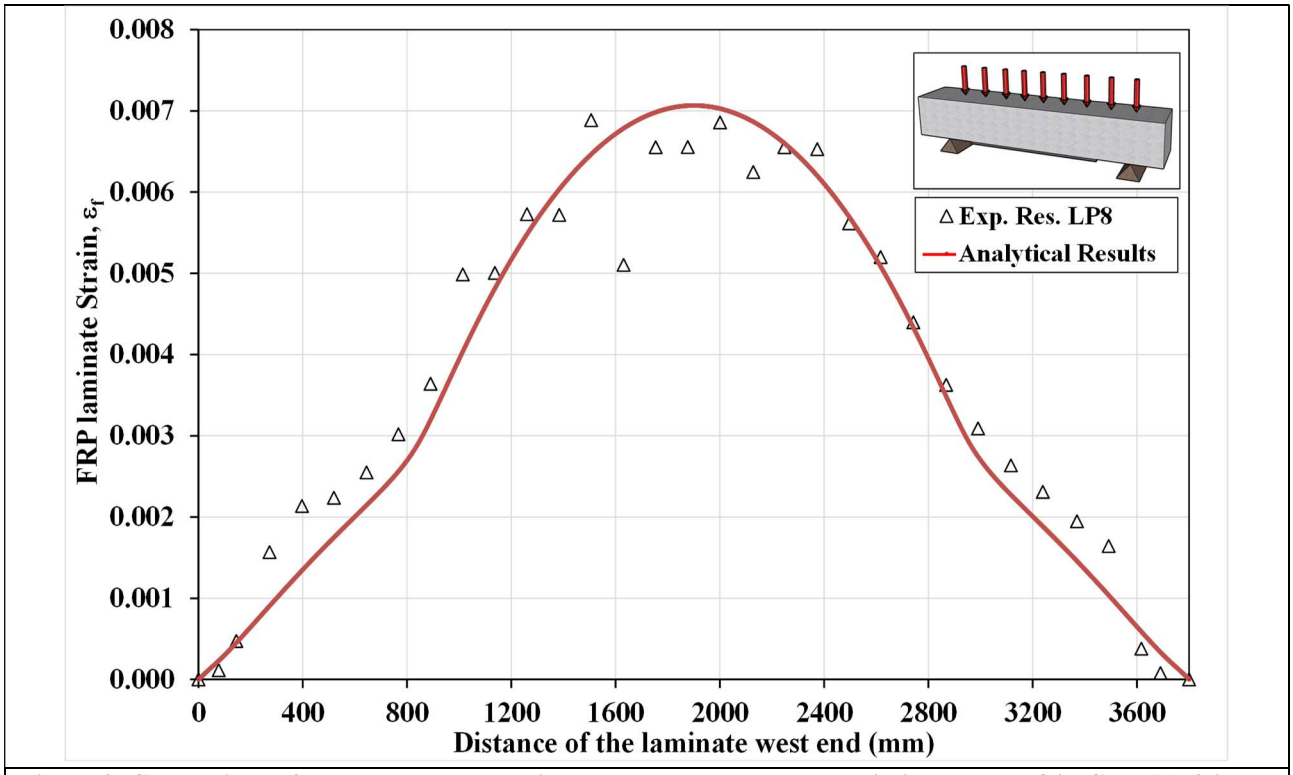

Figure 9. Comparison of computed and experimentally measured FRP strain in Beam LP8 in Case (c) [36].

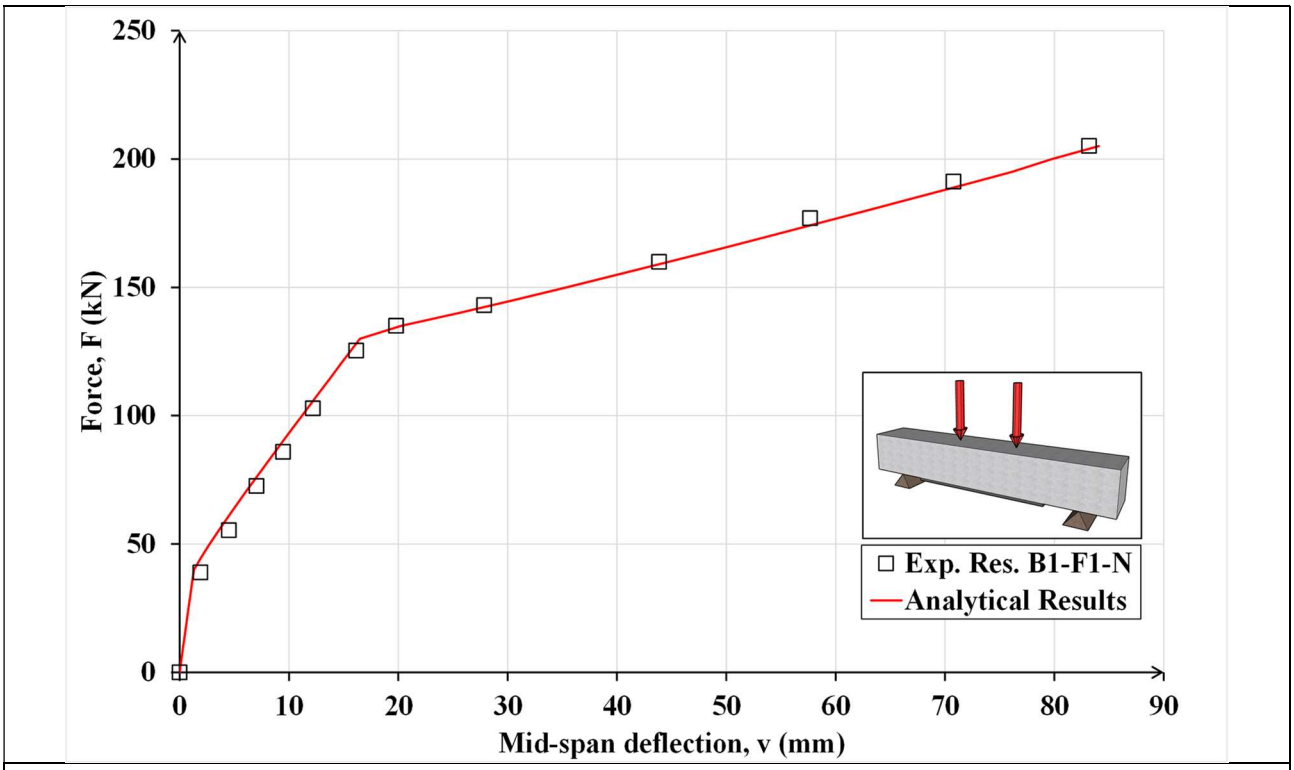

Figure 10: Comparison of computed and experimentally measured force vs. mid-span displacement curve of beam B1F1N in Case (d) [5].

Fig. 10 shows the force vs. mid-span displacement curve for the T-beam tested in Case (d). It was tested in four-point bending and was designated by the original investigators as B1-F1-N.

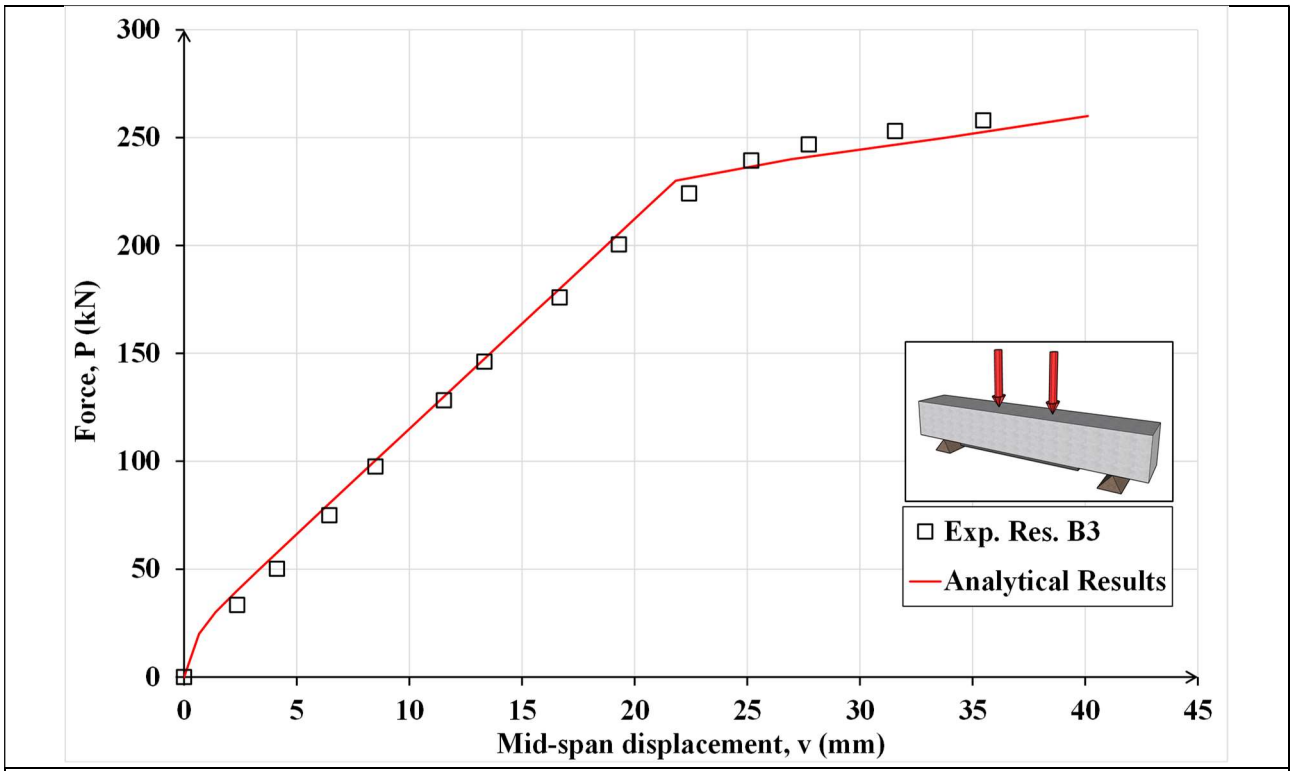

Figure 11: Comparison of computed and experimentally measured force vs. mid-span displacement curve of beam B3 in Case (e) [37].

Fig. 11 shows the force vs. mid-span displacement curve for the beam tested in Case (e). It was tested in four-point bending and was designated by the original investigators as B3.

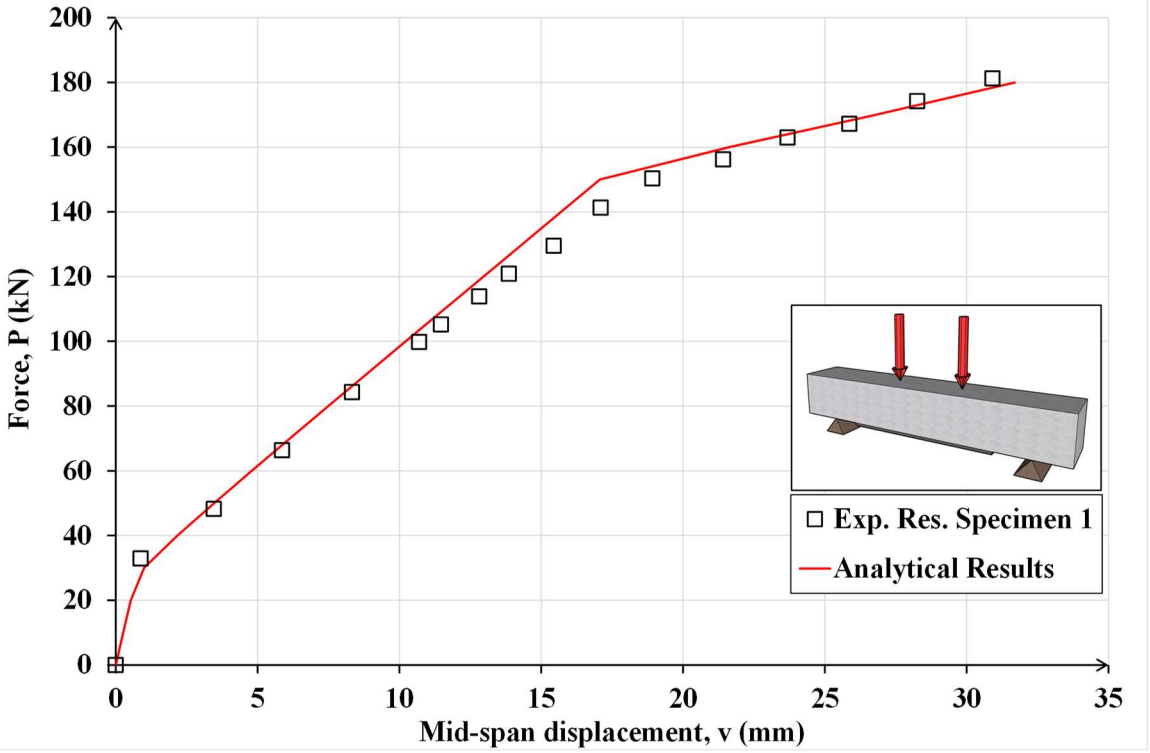

Figure 12: Comparison of computed and experimentally measured force vs. mid-span displacement curve of beam Specimen 1 in Case (f) [38].

Finally, Fig. 12 shows the force vs. mid-span displacement curve for the beam tested in Case (f). It was tested in four-point bending and was designated by the original investigators as Specimen 1.
It is clear from the above comparisons that the proposed method can accurately predict the above RC-retrofitted beams response at all loading stages up to their failure. As these beams have different loading and geometries, the comparisons demonstrate the robustness and accuracy of the method.

Conclusions

A new and refined method of analysis based on nonlinear beam theory is presented to trace the full nonlinear response and debonding load of FRP retrofitted RC beams. Based on results of the analysis, the following conclusions are reached:

(1) It is possible to formulate the governing equations of an FRP retrofitted RC beam in terms of its curvature, including the effects of interfacial slip at the FRP-concrete interface.
(2) It is sufficient to idealize the retrofitted RC section moment-curvature relationship by a trilinear curve, which accounts for the uncracked, cracked-unyielded and cracked-yielded states of the cross-section.
(3) The idealized curve can be easily established by using the suggested procedure in this investigation.
(4) The proposed method can be used to model statically determinate beams with symmetric cross-section subjected to any type of loading.

(5) Based on the several cases analyzed, including rectangular and T-beams beams, subjected to uniform loading or four-point bending, the model can predict accurately the RC beams full load-deflection curve, the debonding load and the strain in the FRP at all loading stages.

Acknowledgments

The first two authors are grateful to the State Administration of Foreign Experts of China, the Tianjin Municipal Government and Nankai University for their financial support of this research.

References

[1] Mosallam A S, Nasr A. Structural performance of RC shear walls with post-construction openings strengthened with FRP composite laminates. Composites Part B: Engineering 2017; 115: 488-504.

[2] Ascione F, Lamberti M, Napoli A, Realfonzo R. SRP/SRG strips bonded to concrete substrate: Experimental characterization. American Concrete Institute, ACI Special Publication 2018, 326.

[3] Carloni C, Ascione F, Camata G, De Felice G, De Santis S, Lamberti M, Napoli A, Realfonzo R, Santandrea M, Stievanin E, Cescatti E, Valluzzi MR. An overview of the design approach to strengthen existing reinforced concrete structures with SRG. American Concrete Institute, ACI Special Publication 2018, 326.

[4] Ascione F, Lamberti M, Napoli A, Razaqpur G, Realfonzo R. An experimental investigation on the bond behavior of steel reinforced polymers on concrete substrate, Composite Structures 2017; 181: 58–72.

[5] Mostafa A B, Razaqpur A G. A nonlinear model for predicting intermediate crack-induced debonding in FRP-retrofitted beams in flexure. Composite Structure 2017; 176: 268-280.

[6] ACI 440.2R. Guide for the Design and Construction of Externally Bonded FRP Systems for Strengthening Concrete Structures. Farmington Hills, MI (USA): ACI, American Concrete Institute; 2017.

[7] CAN/CSA-S806-12. Design and Construction of Building Structures with Fibre reinforced Polymers. Standard by Canadian Standards Association, 2012.

[8] Japan Society of Civil Engineers (JSCE). Recommendation for Design and construction of Concrete Structures Using Continuous Fiber Reinforcing Materials", Concrete Engineering Series No. 23, Tokyo, Japan, 1997.

[9] Fib (CEB-FIP) Bulletin 14. Externally Bonded FRP Reinforcement for RC Structures – technical report, fédération internationale du béton, Lausanne, 2001.

[10] Advisory Committee on Technical Recommendations for Constructions, Italian National Research Council CNR DT200 R1/2013. Guide for the Design and Construction of Externally Bonded FRP Systems for Strengthening Existing Structures, Rome, 2013.

[11] Mostafa A B, Razaqpur A G. A Novel Anchor for Preventing Premature Debonding of Externally Bonded FRP Laminates from Concrete, J. of Composites in Construction 2013; 17: 641-650.

[12] Pan JL, Chung TCF, Leung CKY. FRP debonding from concrete beams under various load uniformities. Adv Struct Eng 2009;12: 807-19.

[13] Robert T M. Approximate Analysis of Shear and Normal Stress Concentration in Adhesive Layer of Plated RC Beams, Structural Engineer 1989; 67: 228-233.

[14] Malek A M, Sadaatmanesh H, Ehsani M R. Prediction of Failure Load of RC Beams Strengthened with FRP Plate due to Stress Concentration at the Plate End, ACI Struct. J 1998; 95: 145-152.

[15] Rabinovitch O, Frostig Y. Closed-form High-order Analysis of RC Beams Strengthened with FRP Strips. J. Compos. Constr. 2000; 4: 65–74.

[16] Ascione L, Feo L. Modeling of composite/concrete interface of RC beams strengthened with composite laminates. Composites Part B: Engineering 2000; 31: 535-540.

[17] El-Mihilmy M, Tedesco J. Prediction of Anchorage Failure for Reinforced Concrete Beams Strengthened with Fiber-Reinforced Polymer Plates, ACI Struct. J 2001, 301-314;

[18] Youssef M A. Analytical Prediction of the Linear and Nonlinear Behavior of Steel Beams Rehabilitated Using FRP Sheets, J. Eng. Struct 2006, 28: 903-11;

[19] Faella C, Martinelli E, Nigro E. Formulation and Validation of a Theoretical Model for Intermediate Debonding in FRP-strengthened RC Beams. Composite Part B: Engineering 2006, 39: 645-655.

[20] Attari N, Amziane S, Chemrouk M. Flexural strengthening of concrete beams using CFRP, GFRP and hybrid FRP sheets. Construction and Building Materials 2012; 37: 746-757.

[21] Triantafyllou G G, Theodoros C. Rousakis T C, Karabinis A I. Analytical assessment of the bearing capacity of RC beams with corroded steel bars beyond concrete cover cracking. Composites Part B: Engineering 2017; 119:132-140.

[22] Mostafa A B, Razaqpur A G. A Finite Element Model for Predicting Post-delamination Behavior of FRP-retrofitted Beams in Flexure. Construction and Building Materials 2017, 131: 195-204.

[23] Dias S J E, Barros J A O, Janwaen W. Behavior of RC beams flexurally strengthened with NSM CFRP laminates. Composite Structures 2018; 201: 363-376.

[24] Koaik A, Bel S, Jurkiewiez B. Experimental tests and analytical model of concrete-GFRP hybrid beams under flexure. Composite Structures 2017; 15:192-2010.

[25] Bencardino F, Condello A. Reliability and adaptability of the analytical models proposed for the FRP systems to the Steel Reinforced Polymer and Steel Reinforced Grout strengthening systems. Composites Part B: Engineering 2015;76:249-259.

[26] Sharaky I A,Torres L, Sallam H E M. Experimental and analytical investigation into the flexural performance of RC beams with partially and fully bonded NSM FRP bars/strips. Composite Structures 2015:122:113-26.

[27] Taljsten B. Strengthening of beams by plate bonding. Journal of Materials in Civil Engineering 1997: 205-2012.

[28] Smith S T , Teng J G. Interfacial stresses in plated beams. Engineering Structures 2001; 23: 857–871.

[29] Rabinovitch O. Fracture-mechanics failure criteria for RC beams strengthened with FRP strips––a simplified approach. Composite Structures 2004; 64: 479–492.

[30] Al-Zaid R Z , Al-Negheimish A I, Al-Saawani M A, El-Sayed A K. Analytical study on RC beams strengthened for flexure with externally bondedFRP reinforcement. Composites: Part B 2012; 43:129–141.

[31] Rezazadeh M, Barros J, Costa I. Analytical approach for the flexural analysis of RC beams strengthened with prestressed CFRP. Composites: Part B 2015;73: 16–34.

[32] Ascione F. Mechanical behaviour of FRP adhesive joints: a theoretical model. Composites Part B: Engineering 2009; 40: 116-124.

[33] Ascione F, Lamberti M, Napoli A, Razaqpur AG, Realfonzo R. Modeling SRP-concrete interfacial bond behaviour strength. Engineering Structures 2019; 187: 220–230.

[34] Cosenza E, Manfredi G, Realfonzo R. Behaviour and Modeling of bond FRP rebars to concrete. J Compos Constr 1997;1(2):40-51.

[35] Mazzotti C, Savoia M. Experimental tests on intermediate crack debonding failure in FRP-strengthened RC beams. Adv Struct Eng 2009;12(5):701–13.

[36] Fu B, Teng G, Chena G M, Chena JF , Guoa Y C. Effect of load distribution on IC debonding in FRP-strengthened RC beams: Full-scale experiments. Composite Structures 2018; 188: 483-496.

[37] Maalej M, Leong K S. Effect of beam size and FRP thickness on interfacial shear stress concentration and failure mode of FRP-strengthened beams. Composites Science and Technology 2005;65:1148–1158.

[38] Spyrakos C C, Raftoyiannis I G, Credali L and Ussia J. Experimental and Analytical Study on Reinforced Concrete Beams in Bending Strengthened with FRP. The Open Construction and Building Technology Journal 2014; 8: 153-163.

[39] Wight J K, MacGregor J G. Reinforced Concrete: Mechanics and Design, Prentice Hall, N J, 2009.

[40] Okamura H, Maekawa K, Sivasubramaniyam S. Verification of modeling for reinforced concrete finite element. Finite element analysis of reinforced concrete structures. ASCE 1985:528–43.

Appendix A – Construction of the moment-curvature and resultant force-extreme fiber relationships

The moment-curvature (M-χ) and resultant force-extreme fiber concrete strain (F_c-ε) diagrams for an FRP retrofitted reinforced concrete (RC) section are shown in Figure 4 (a) and (b), respectively. These are obtained for a section undergoing slip at its interface with the FRP and depend on the location of the section along the beam, thus is different from the conventional moment-curvature relationship for a RC section, which is function of the section properties only.

The construction of these diagrams requires the tensile and compressive stress-strain relationships of the retrofitted beam constituent materials. These relationships for the concrete and steel are shown in Fig. A.1, while the FRP is assumed to behave linear-elastically, with zero compressive strength. The concrete in compression is modelled by the Thornenfeld et al. [39] proposed stress-strain relationship, represented by Eq. (A.1), which is suitable for concrete strengths up to 100 MPa.

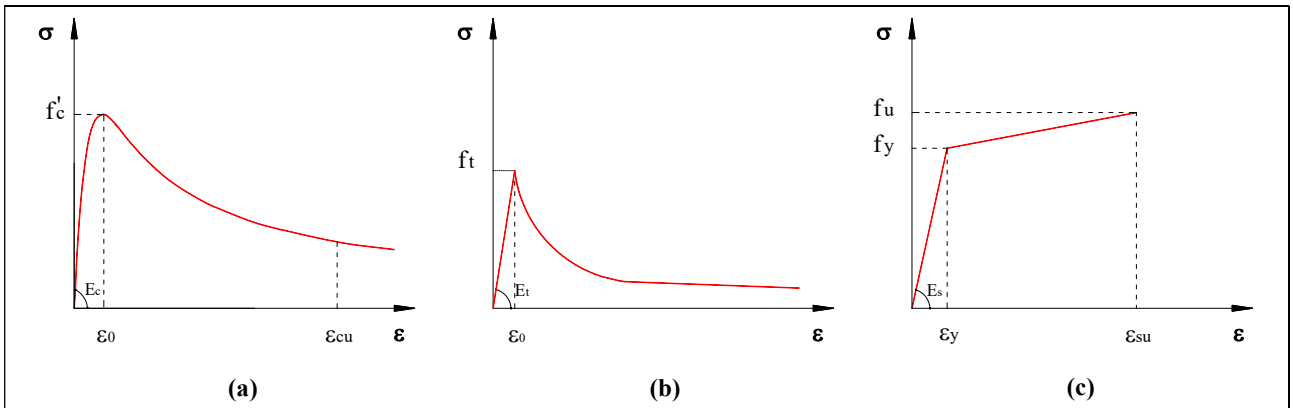

Figure A.1:Stress-Strain Relationship: a) Concrete in compression, b) Concrete in tension; c) Steel bars

$$\frac{\sigma_c}{f_c'} = \frac{n\left(\frac{\varepsilon_c}{\varepsilon_0}\right)}{n-1+\left(\frac{\varepsilon_c}{\varepsilon_0}\right)^{nk}} \qquad \text{(A.1)}$$

where σ_c and ε_c are the concrete compressive stress and strain, respectively, f_c' is the peak stress obtained from a cylinder test, ε_0 the strain corresponding to f_c', n is a curve-fitting factor equal to $\frac{E_c}{(E_c - E_c')}$, E_c is the initial tangent Young modulus, E_c' is equal to $\frac{f_c'}{\varepsilon_0}$ and k is a factor to control the slopes of the ascending and descending branches of the stress-strain curve, with k = 1.0 for $\frac{\varepsilon_c}{\varepsilon_0} \leq 1.0$ and $k > 1.0$ for $\frac{\varepsilon_c}{\varepsilon_0} > 1.0$. For the choice of the appropriate n and k values for a specific concrete, reference should be made to the above cited source [39].

The concrete in tension is modelled as linear elastic before cracking and as a strain-softening material after cracking as illustrated in Fig. (A.1b) and expressed by Eq. (A.2a) and (b), respectively.

$\sigma_{ct} = E_t \varepsilon_{ct}$ for $\varepsilon_c \le \varepsilon_{to}$ with $E_t = \frac{E_c}{2}$, $\varepsilon_{to} = \frac{f_t}{E_t}$	(A.2a)
$\sigma_{ct} = f_t \left(\frac{\varepsilon_{ct}}{\lvert \varepsilon_{to} \rvert} \right)^c$ for $\varepsilon_{ct} > \varepsilon_{to}$	(A.2b)

where E_t is the elastic modulus of concrete in tension, f_t is the absolute value of its tensile strength and ε_{to} is its corresponding strain. The power c in Eq. (A.2b) controls the shape of the softening branch of curve. Its value will depend on the RC section geometric and mechanical properties. Typically, it ranges between 0.2 and 0.6 [40], but further discussion is beyond the scope of this study. For the steel reinforcement, a typical bilinear stress-strain relationship is adopted as in Fig. A.1(c), which is expressed by

$\sigma_s = E_s \varepsilon_s$ for $\varepsilon_s \le \varepsilon_y$ with, $\varepsilon_y = \frac{f_y}{E_s}$	(A.3a)
$\sigma_s = \frac{f_u - f_y}{\varepsilon_{su} - \varepsilon_y} \varepsilon_s$ for $\varepsilon_y < \varepsilon_s < \varepsilon_{su}$	(A.3b)

where E_s, f_y, ε_y, f_u and ε_{su} are the elastic modulus, yield stress, yield strain, ultimate strength and corresponding ultimate strain of the reinforcing steel.

The process of determining the moment-curvature response begins with the division of the RC section into *n* concrete and steel layers, Fig. A.2, with layer *i* having thickness h_i *(i=1, n)*. The value of *n* is selected by the analyst, but *n*=10 generally suffices. Thereafter, the procedure proceeds as follows:

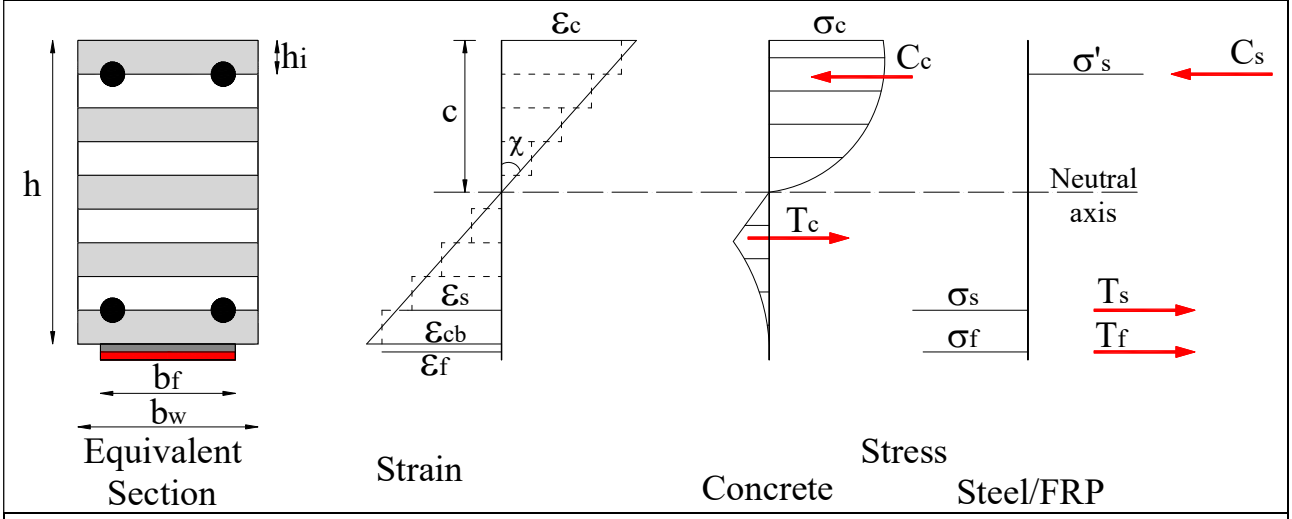

Figure A.2: Fiber discretization of the RC beam cross-section.

(i) Select a small value for ε_{cb} at the extreme tension fiber of the section

(ii) Assume the depth of the neutral axis, *c*

(iii) Apply full strain compatibility to compute the strain ε_i in any concrete or steel layer *i*,

(iv) Use ε_i and the constitutive relations in Fig. A.1, determine for any layer *i* its stress σ_i

(v) At the section of interest, determine the FRP strain, ε_f, using Eq. (A.4a) if slip $\lambda \le \lambda_o$ and Eq (A.4b) if $\lambda_o < \lambda \le \lambda_{\max}$

(vi) Determine the stress in the FRP, $\sigma_f = E_f \varepsilon_f$, corresponding to the strain in step (v)

(vii) Determine the force $F_i = A_i \sigma_i$ in each layer *i,* designating compression forces as C_i and tension forces as T_i. Note A_i is the cross-sectional area of layer *i*

(viii) Check equilibrium. Is $\left(\sum_i^n C_i - \sum_i^m T_i\right) \approx 0$, where *n* and *m* are the number of compression and tension forces, respectively, acting on the section. If the difference between the two set of forces is less than or equal to a preset convergence tolerance, go to step (xi), otherwise continue.

(ix) Go to step (ii) and revise the value of *c*

(x) Continue steps (iii) to (viii) until the selected convergence tolerance is satisfied

(xi) Once convergence is achieved, compute the moment M_c resisted by retrofitted RC section corresponding to the selected ε_{ct} in step (i) $M_c = \sum_{i=1}^{n} M_i = \sum_{i=1}^{n} F_i d_i$ and $F_c = \sum_{i=1}^{n} F_i$ where *n* is the total number of layers and d_i is the distance of force *i* from the axis going through the point of application of the compressive force (C_c) in the concrete. The sign of the forces and their moment arms must be duly observed.

(xii) The curvature $\chi = \dfrac{\varepsilon_{cb}}{(h-c)}$

(xiii) The set of χ_c and M_c thus obtained gives one point on the M_c-χ_c curve while the companion set of ε_{cc} and F_c give a point on the F_c-ε_{cc} diagram.. Additional points can be obtained by selecting different values for ε_{cc}.

$\varepsilon_f(x) = A_1 e^{w_1 x} + B_1 e^{-w_1 x} + \varepsilon_c$ with $w_1^2 = \dfrac{k_s}{t_f E_f}$ if $\lambda \le \lambda_0$	(A.4a)
$\varepsilon_f(x) = A_2 \cos(w_2 x) + B_2 \sin(w_2 x) + \varepsilon_c$ with $w_2^2 = \dfrac{k_b}{t_f E_f}$ if $\lambda_0 < \lambda \le \lambda_0$	(A.4b)
$\varepsilon_f\left(\dfrac{L_f}{2}\right) = 0$, $\varepsilon_f(0) = \varepsilon_c$ (no slip)	(A.4c)

For the construction of the trilinear curves in Fig. 4(a) and (b), select only the following three ε_{cb} values: $\varepsilon_{cb} = \varepsilon_{ct}$, $\varepsilon_{cb} = \dfrac{h-c}{d_s - c}\varepsilon_y$ and $\varepsilon_{cb} = \dfrac{h-c}{c}\varepsilon_{cu}$, where d_s is the effective depth of the steel layer that is located closest to extreme tension fiber of the section. It is also advisable to compute the moment corresponding to FRP rupture, i.e. ε_f = FRP rupture strain.